ACSNANO
www.acsnano.org
ARTICLE

Tribotronic Tuning Diode for Active Analog Signal Modulation

Tao Zhou,[†,§] Zhi Wei Yang,[†,§] Yaokun Pang,[†] Liang Xu,[†] Chi Zhang,[*,†] and Zhong Lin Wang[*,†,‡]

[†]Beijing Institute of Nanoenergy and Nanosystems, National Center for Nanoscience and Technology (NCNST), Chinese Academy of Sciences, Beijing 100083, People's Republic of China

[‡]School of Materials Science and Engineering, Georgia Institute of Technology, Atlanta, Georgia 30332, United States

Supporting Information

ABSTRACT: **Realizing active interaction with external environment/stimuli is a great challenge for current electronics. In this paper, a tribotronic tuning diode (TTD) is proposed by coupling a variable capacitance diode and a triboelectric nanogenerator in free-standing sliding mode. When the friction layer is sliding on the device surface for electrification, a reverse bias voltage is created and applied to the diode for tuning the junction capacitance. When the sliding distance increases from 0 to 25 mm, the capacitance of the TTD decreases from about 39 to 8 pF. The proposed TTD has been integrated into analog circuits and exhibited excellent performances in frequency modulation, phase shift, and filtering by sliding a finger. This work has demonstrated tunable diode and active analog signal modulation by tribotronics, which has great potential to replace ordinary variable capacitance diodes in various practical applications such as signal processing, electronic tuning circuits, precise tuning circuits, active sensor networks, electronic communications, remote controls, flexible electronics, *etc.***

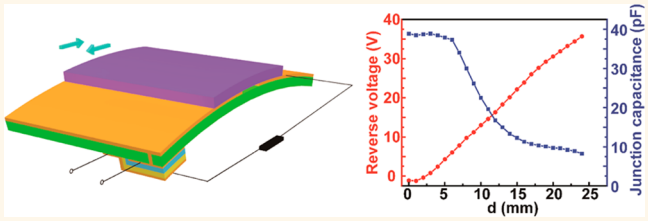

KEYWORDS: *tribotronics, triboelectric nanogenerator, sliding electrification, tuning diode, signal modulation*

With the increasing demands for intelligent electronic devices, such as for instant messaging, smart wearable devices, personal health monitoring, and sensor networks, developing functional interactive devices for users has been of great significance.[1−7] Analog signal modulation is the processing and transformation of a continuous time signal, which plays a vital role for functional electronics. However, due to the lack of a direct interaction mechanism between the external environment/stimuli and analog devices, the analog signals can only be electrically modulated in conventional circuits, which makes the active analog signal modulation for human−machine interaction and flexible electronics highly desirable.

Since its invention in 2012, the triboelectric nanogenerator (TENG),[8−17] which is based on the coupling of triboelectrification and electrostatic induction, has been proven to be a cost-saving way to convert mechanical energy into electricity. With the advantage of high voltage, the TENG is very suitable for driving a capacitive load and developing triboelectric voltage-controlled devices.[18,19] Besides, by using the electrostatic potential generated from the TENG to modulate electronics, a new field of tribotronics was proposed by coupling triboelectricity and semiconductors.[20,21] Tribotronics has a self-generated inner controlling signal by an external mechanical stimulus and provides an active human−machine interaction method. To date, various tribotronic devices have been developed such as electro-mechanical coupled logic circuits,[22] contact-gated light-emitting diodes,[23] touch memory,[24] enhanced photocells,[25] adjustable photodetectors,[26] tactile switches,[27] force-pads,[28] and sensing arrays.[29] All of these tribotronics are based on the theoretical model of a tribotronic transistor,[30,31] in which the electrostatic potential by triboelectrification is applied on a MIS capacitor for modulating charge carrier transport. Beyond that, as a capacitive load, the p−n junction capacitor in a diode could also be tuned by the tribopotential, which may derive a different tribotronic device and provide a solution for active analog signal modulation.

In this paper, a flexible tribotronic tuning diode (TTD) is proposed by combining a variable capacitance diode with a TENG in free-standing mode. The capacitance of the TTD can be tuned by the sliding motion of a polymer film. By integrating the TTD into analog circuits, the frequency modulation, phase shift, and filtering of analog signals were successfully achieved by sliding a finger. Different from previous tribotronic transistors, this work demonstrates a tribotronic diode for active analog signal modulation. Moreover, apart from the three applications demonstrated in this paper, in fact, the TTD can be utilized instead of ordinary tunable capacitors in various applications, such as high-pass filtering, band-pass filtering, band elimination filtering, active filter circuits, TV tuning circuits, amplitude

Received: November 5, 2016
Accepted: December 21, 2016
Published: December 21, 2016

DOI: 10.1021/acsnano.6b07446
ACS Nano 2017, 11, 882−888

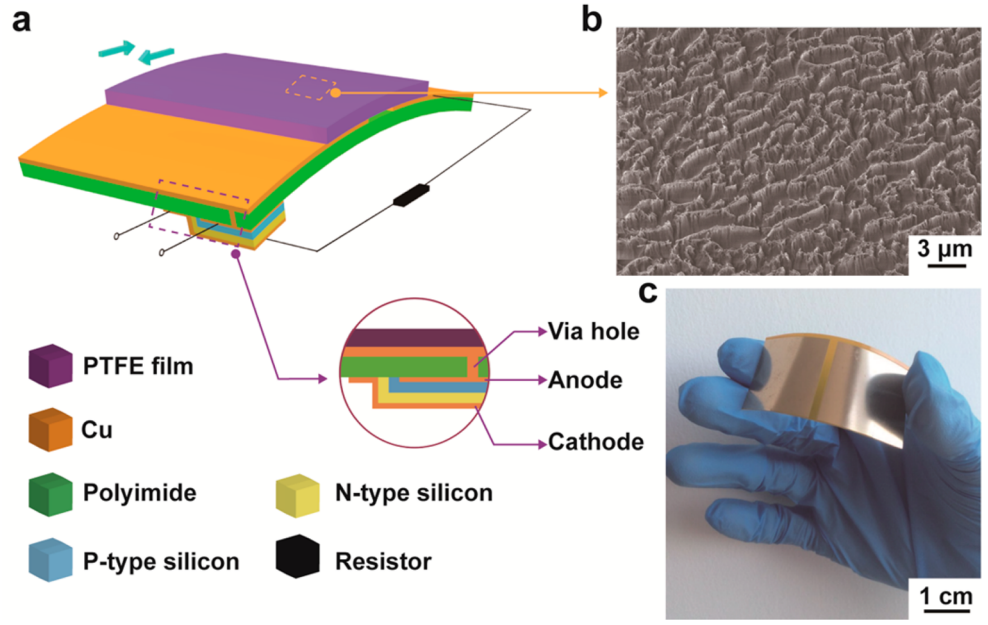

Figure 1. Structure of a representative TTD. (a) Schematic illustration of the TTD. Inset: Cross-section configuration of the TTD, showing an electrical connection between the TENG in free-standing mode and a p−n junction by a via hole. (b) Scanning electron microscopy image of nanostructures on the surface of the contact electrification layer made of PTFE film. (c) Photograph of the TTD.

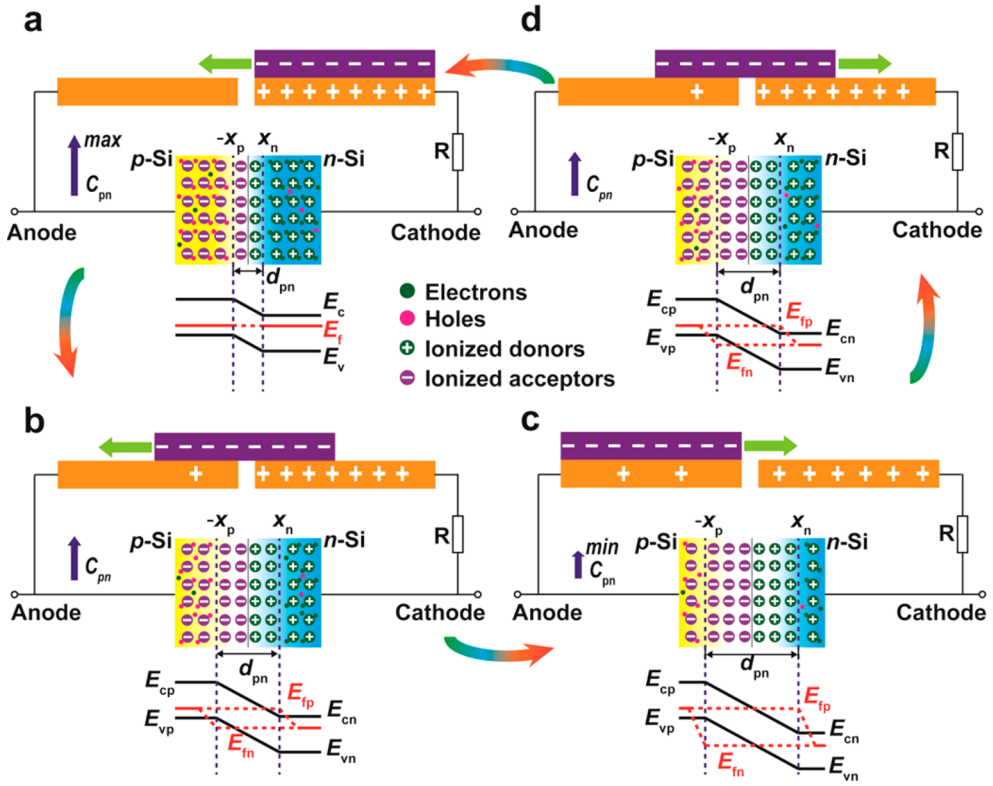

Figure 2. Proposed working mechanism of the TTD and band structures of the p−n junction at four positions. (a) Initial state when the PTFE film contacts the right Cu pad and the corresponding band stucture where the Fermi level is aligned. At this moment, the junction capacitance (C_{pn}) has a maximum value. (b) State when the PTFE film moves to a left position. A reverse voltage is applied to the p−n junction; the depletion zone width (d_{pn}) increases, whereas the C_{pn} decreases. (c) Sliding the PTFE film to fully cover the left Cu pad maximizes the d_{pn}, minimizes the C_{pn}, and splits the Fermi level to a maximum value. (d) Reverse changing process of all d_{pn}, C_{pn}, and Fermi level when the PTFE electrification film slides backwards.

limiting circuits, FM modulation circuits, *etc*. Therefore, the TTD may have potential applications in smart wearable devices, signal processing, active sensor networks, electronic communications, and remote controls.

DOI: 10.1021/acsnano.6b07446
ACS Nano 2017, 11, 882−888

RESULTS AND DISCUSSION

Structure of the TTD. Figure 1 demonstrates the basic structure of the TTD. It mainly consists of a flexible polyimide substrate, two Cu pads (20 mm × 25 mm for each one), a free-standing polytetrafluoroethylene (PTFE) film (20 mm × 25 mm), a variable capacitance diode, and a resistor, as shown in Figure 1a. The two Cu pads are deposited on the top of the flexible polyimide substrate, and the diode made of a silicon-based p−n junction is constructed on the bottom layer. The anode and the cathode are in connection with the p-type and n-type sides of the diode, respectively. Through the designed via hole, the left Cu pad is also connected to the anode, which is depicted in the cross-sectional inset. In order to optimize the triboelectrification between the two materials, the surface of the PTFE film is modified *via* inductive coupling plasma (ICP) to create nanostructures (Figure 1b), which can enhance the surface triboelectric charge density of the PTFE film. A well-designed TTD is presented in Figure 1c (the detailed fabrication process is introduced in the Methods).

Working Mechanism of the TTD. The working mechanism of the TTD is elaborated in Figure 2. The Cu pad serves as the triboelectric material and also the working electrode. As can be seen in Figure 2a, when the PTFE film fully contacts the right-hand Cu pad, equal negative and positive charges are induced on the surfaces of the PTFE film and the Cu pad, respectively, due to their difference in triboelectric polarity. Because the positive triboelectric charges completely balance out the negative counterpart in this circumstance, there is no electrical potential difference applied to the p−n junction and no charges flowing in the entire structure. Besides, the Fermi level in the energy band diagram in Figure 2a is horizontally aligned, and a barrier zone with a width of d_{pn} is built in the p−n junction. Hence, the tunable capacitance of the diode can be expressed as

$$C = kS/d_{pn} \tag{1}$$

where k is the dielectric constant, S is the surface area of the p−n junction, and d_{pn} represents the barrier width. When the PTFE film moves laterally along the Cu electrode upon a sliding force (Figure 2b), partial positive charges on the right-hand electrode will lose constraints because of the decreased contact area and will have a tendency to flow from the right-hand electrode to the left one, resulting in a negative electrical potential applied to the p−n junction. This potential will lead to the Fermi level splitting, where the electron quasi-Fermi level is lowered and the hole quasi-Fermi level is raised. The d_{pn} is also widened as a result of the reverse bias voltage to the p−n junction. According to eq 1, the increased d_{pn} results in the decrease of the junction capacitance. Further increase of the sliding distance to fully overlap with the left-hand electrode (Figure 2c) will maximize the applied reverse bias voltage. Accordingly, the Fermi level is split to a maximum value, and the junction capacitance reaches the minimum. When the PTFE film slides backwards (Figure 2d), the reverse bias voltage is reduced, thus causing the reduction of the d_{pn}. In this scenario, the capacitance of the p−n junction will eventually recover to the maximum when the PTFE film is overlapped with the right-hand electrode again. Based on that mentioned above, the junction capacitance can be effectively tuned by an external force, which is of great value in later discussion of analog signal modulation.

Electrical Characterization of the TTD. To better evaluate the performance of the TTD, its electric characterizations were systematically studied, as depicted in Figure 3. Figure 3a(i,ii)

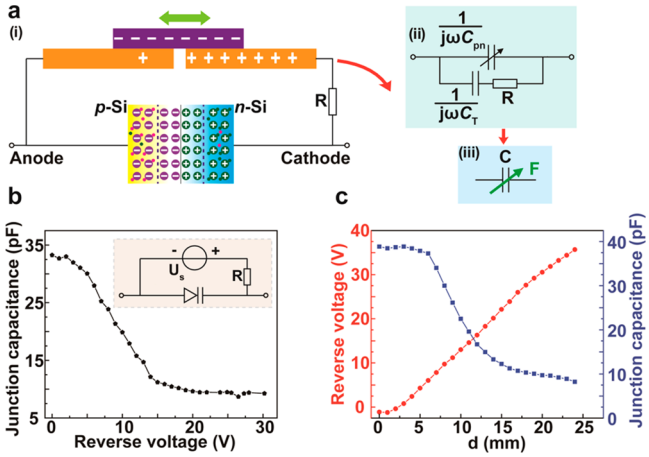

Figure 3. Equivalent circuit and electrical characterization of the TTD. (a) Equivalent circuit diagram of the TTD and the simplified symbol after mathematical derivation. (b) Junction capacitance as a function of the electrically applied reverse voltage. Inset: Equivalent circuit when the TENG is replaced by a power source. (c) Output reverse voltage from the TENG and the junction capacitance as a function of the sliding distance of the PTFE film.

shows the schematic illustration and the equivalent circuit diagram of the TTD, respectively. Here, the diffusion capacitance of the p−n junction could be reasonably ignored, originating from its exponential reduction as the reverse bias voltage increased, which caused the total capacitance of the p−n junction to be equivalent to a barrier capacitance C_{pn}. According to previous theoretical study of the TENG in free-standing mode,[32,33] the impedance of the TENG could be equivalent to an inherent capacitance C_T. The equivalent impedance of the TTD unit is shown in Figure 3a(ii). Assuming that the whole equivalent impedance of the TTD unit was Z, it could be expressed as follows:

$$Z = \left(R + \frac{1}{j\omega C_T}\right) // \frac{1}{j\omega C_{pn}} = \frac{j\omega C_T R + 1}{j^2\omega^2 C_T C_{pn} R + j\omega C_{pn} + j\omega C_T} \tag{2}$$

where R represented the series resistor, j was the imaginary unit, and ω was the angular frequency. The resistor R was used to reduce the influence of the inherent TENG capacitance C_T on the whole equivalent impedance of the TTD unit. When the resistance of R was very high (here, it is 10 MΩ) and the TTD worked at low frequency, the expressions without R could be ignored, thus eq 2 could be simplified as

$$Z \approx \frac{j\omega C_T R}{j^2\omega^2 C_T C_{pn} R} = \frac{1}{j\omega C_{pn}} \tag{3}$$

Therefore, the impedance of TTD was approximately equal to that of a capacitor C_{pn}. Because the value of C_{pn} was determined by the output voltage of TENG, as elaborated in Figure 2, the TTD could be equivalent to an external force-controlled tunable capacitor, as shown in Figure 3a(iii).

In order to fully understand the electrical characteristic of the TTD, the relationship between the electrically applied reverse voltage and the capacitance of the p−n junction was first studied, as plotted in Figure 3b, where the reverse voltage was applied by a variable voltage source U_s instead of the TENG, as depicted in

DOI: 10.1021/acsnano.6b07446
ACS Nano 2017, 11, 882−888

the inset of Figure 3b. It could be observed that the junction capacitance decreased from 33 to about 8 pF as the reverse voltage increased from 0 to 30 V. Notably, once the reverse voltage surpassed a critical value of 16 V, the junction capacitance displayed a slow decline. Figure 3c demonstrated the output reverse voltage from the TENG and the junction capacitance as a function of the sliding distance of the PTFE film. As shown in Figure 3c, the output reverse voltage from the TENG was proportional to the sliding distance, while the junction capacitance declined with the increase of the sliding distance and a sharp decline started from about 5 mm. All of these data strongly verified the working principle of the TTD illustrated in Figure 2. When the sliding distance reached a value of about 15 mm, slight changes of the capacitance would be seen, which meant that even if the output voltage of the TENG continued to increase, the TTD's capacitance only underwent a slow decrease. This result was in good agreement with the analysis in Figures 2 and 3b, thus proving that the TENG could be a promising candidate to control the tunable diode, in place of the voltage source.

Application of the TTD for Active Analog Signal Modulation. First, the TTD was applied to analog signal frequency modulation (Figure 4). The schematic circuit diagram of the frequency modulation by TTD is shown in Figure 4a, which consists of an LC parallel resonant circuit and an oscillator. The frequency of the output signal f_{out} was determined by the resonance frequency (denoted as f_0) of the LC circuit:

$$f_0 = \frac{1}{2\pi\sqrt{LC_{pn}}} \tag{4}$$

where the inductor L was 330 nH. Therefore, the frequency of f_{out} was solely determined by the capacitance C_{pn} of the TTD, namely, the sliding distance of the PTFE film. The relationship between the output signals and the sliding distance was investigated. With three modulation states (d = 0, 10, 25 mm), as shown in the schematics, three sinusoidal waves with different frequencies were acquired and plotted in Figure 4b. When the PTFE film stayed at the initial position, the frequency of the f_{out} presented a minimum value. An evident frequency increase appeared when the sliding distance increased to 25 mm. Figure 4c shows the frequency spectrum of the modulated sinusoidal signal in Figure 4b. Obviously, the frequencies of the three peaks are of 38.0, 65.2, and 81.5 MHz, which correspond to the three sliding distances (0, 10, 25 mm). Figure 4d was the result of a continual sliding and its corresponding frequency distribution of the output signal. The dots in blue are the experimental results, and the curve is the fitted result. The results further confirmed that the TTD was an effective tool to actively modulate the frequency. Video S1 in the Supporting Information dynamically demonstrates the frequency modulation process. It remarkably shows that frequency modulation could be realized by an external sliding motion of a finger, which was distinguished from traditional modulation methods powered by a voltage source. As a supplement to assess the performance of the TTD, the frequency of the output signal was also investigated by using a series of capacitors with different values in place of the TTD, as displayed in Figure S1. The similar changing trends found in Figure S1 and Figure 4d strongly verify the effectiveness of the TTD to work as variable capacitance in analog circuits by an external sliding motion.

To further validate the ability of the proposed TTD to realize active modulation, it was also integrated into an analog circuit to

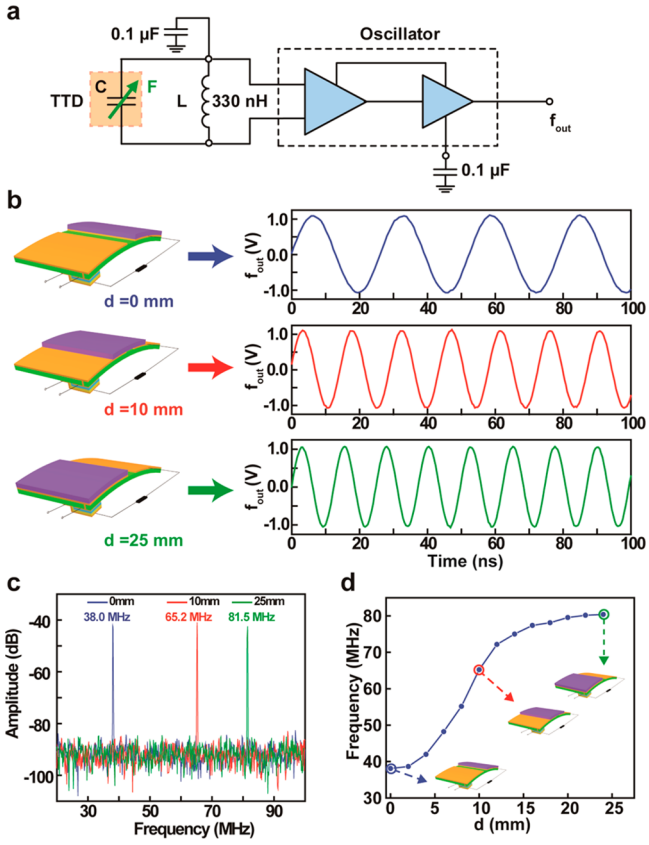

Figure 4. TTD for analog signal frequency modulation. (a) Schematic circuit diagram of the frequency modulation by TTD in conjunction with an LC circuit and an oscillator. (b) Schematics of three modulation states and their corresponding output sinusoidal signals with different frequencies. (c) Amplitude−frequency characteristics of the modulated sinusoidal signal. Three peaks corresponding to the sliding distances were precisely identified. (d) Frequency distribution of the modulated sinusoidal signals when the sliding distance ranged from 0 to 25 mm. Three states were in correspondence to panel b. A frequency modulation range of about 40 MHz was achieved.

tune the signal phase. Figure 5a is the designed circuit composed of an operational amplifier, a TTD, and three resistors R_p with the same value. According to the basic concept of the operational amplifier and the configuration of the circuit, the ratio ($H(j\omega)$) of the output voltage signal (U_{out}) to the input voltage signal (U_{in}) and their phase difference (φ) could be represented as

$$H(j\omega) = \frac{U_{out}}{U_{in}} = \frac{j\omega R_p C_{pn} - 1}{j\omega R_p C_{pn} + 1}$$

$$|H(j\omega)| = \left|\frac{U_{out}}{U_{in}}\right| = \left|\frac{j\omega R_p C_{pn} - 1}{j\omega R_p C_{pn} + 1}\right| = \frac{\sqrt{(j\omega R_p C_{pn})^2 + 1}}{\sqrt{(j\omega R_p C_{pn})^2 + 1}} = 1 \tag{5}$$

$$\varphi = \angle H(j\omega) = -2\arctan(2\pi f R_p C_{pn}) \tag{6}$$

where f is the frequency of the input signal. When f = 10 MHz and R_p = 1.4 kΩ, the calculated phase shift range would be −47.5 to −147.5° with the capacitance varying from 5 to 39 pF. Besides theoretical analysis, the phase modulation by TTD was

DOI: 10.1021/acsnano.6b07446
ACS Nano 2017, 11, 882−888

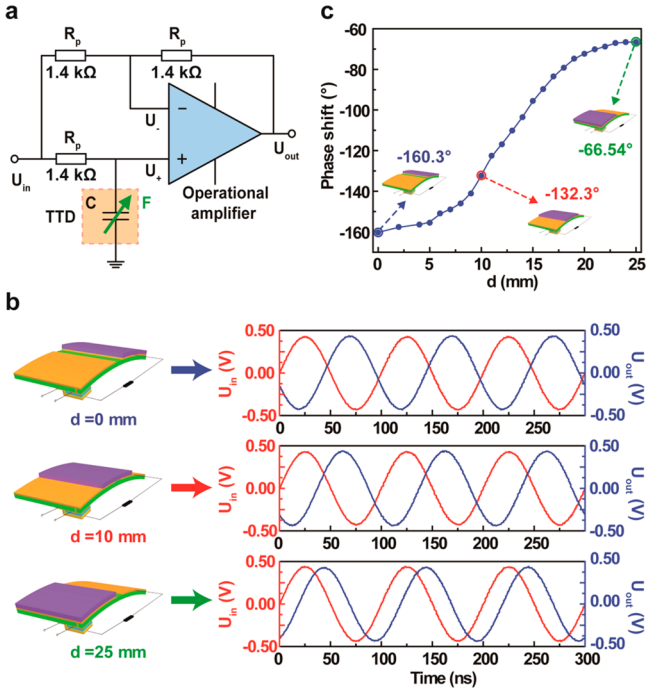

Figure 5. TTD for analog signal phase shift. (a) Schematic circuit diagram of the phase modulation by TTD in conjunction with an operational amplifier. (b) Schematics of three modulation states and their corresponding input and output sinusoidal signals with different phase differences. (c) Phase shift of the output signal as the sliding distance varied from 0 to 25 mm. Three specific values corresponded to the three states shown in panel b.

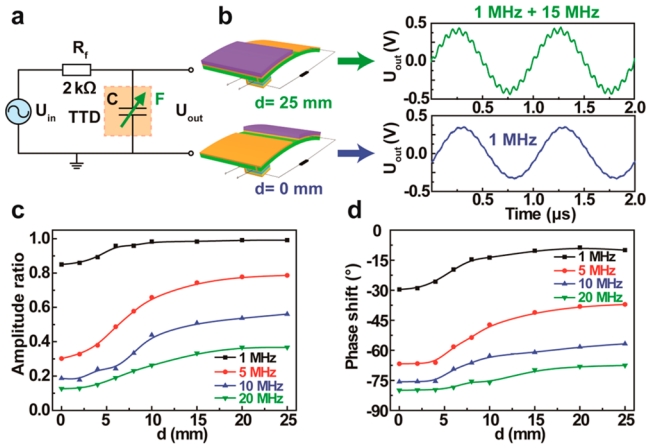

Figure 6. TTD for analog signal filtering. (a) Schematic circuit diagram of the low-pass filtering by TTD. (b) Schematics of two modulation states and their corresponding output sinusoidal signals with different filtering effects. A 1 MHz standard sine wave, along with a 15 MHz disturbance, was selected as the input signals. (c) Amplitude ratio of the output signal to the input signal as a function of the sliding distance at different frequencies. (d) Phase−distance characteristics of the TTD-controlled filtering circuit at different frequencies.

experimentally measured. In this study, the sliding distance of the PTFE film and the corresponding signals were recorded, and three acquired signals were picked out, as graphed in Figure 5b. Initially, a phase difference of −160.3° could be observed without sliding. Then the output signal shifted to the left, and the phase difference gradually diminished to −132.3° (d = 10 mm). Once the sliding distance reached 25 mm, the phase difference decreased to −66.54° (Video S2 in Supporting Information demonstrates the phase shift process). It was noteworthy that, during the sliding process, a phase shift of about 100° was achieved whereas the amplitude of both input and output signals was maintained, thus proving that the experimental results matched well with the formulas derived before. Figure 5c depicts the phase difference as a function of the sliding distance in the whole process, and a continual phase shift could be obtained. The phase shift was then assessed by a series of capacitors with different values, instead of the TTD. Compared with the results obtained in Figure 5c, the experimental curve plotted in Figure S2 had the same changing trend, indicating that there was a good agreement between the two experiments. Therefore, this outcome further substantiated the applicability of the TTD to realize the phase shift in analog circuits, by just sliding a finger.

Besides the aforementioned applications, the subsequently intriguing one is the TTD-based analog signal filtering. Graphed in Figure 6a is the electrical circuit diagram, including the external force-controlled TTD equaled to a tunable capacitor, and a resistor R_f, as depicted in Figure 3a. According to the definition of low-pass filtering, its amplitude−frequency and phase−frequency characteristics could be written as

$$|H(j\omega)| = \left|\frac{U_{out}}{U_{in}}\right| = \left|\frac{\frac{1}{j\omega C_{pn}}}{R_f + \frac{1}{j\omega C_{pn}}}\right| = \frac{1}{\sqrt{1 + (\omega R_f C_{pn})^2}} = \frac{1}{\sqrt{1 + (2\pi f R_f C_{pn})^2}} \quad (7)$$

$$\varphi = \angle H(j\omega) = -\arctan(\omega R_f C_{pn}) = -\arctan(2\pi f R_f C_{pn}) \quad (8)$$

where f is the frequency of the input signal. Two filtering effects based on the TTD circuit are displayed in Figure 6b. A disturbance (15 MHz) superposed on a standard sine wave (1 MHz) was chosen as the input analog signal. When the PTFE film slid to a maximum distance of 25 mm and stayed at this position, the output signal remained nearly unchanged compared to the input signal. However, once the PTFE film slid to the 0 mm position, the curve in blue distinctly demonstrated that the disturbance was heavily suppressed, leaving the output wave almost consisting of the standard sinusoidal signal. Slight fluctuations on the filtered output signal could be attributable to the remains of the disturbance, which could not be completely attenuated. That was because the amplitude of the output 15 MHz disturbance was reduced to about 0.02 times of the original according to eq 7. Figure 6c displays the amplitude ratio of the output signal to the input signal as a function of the sliding distance at different frequencies, which represented the attenuation degree of the input analog signal. Figure 6d showed the phase−distance characteristics of the TTD-controlled filtering circuit at different frequencies, which depicted the phase shift of the output signal relative to the input signal. It could be clearly seen that with a decreased sliding distance and an increased frequency (*e.g.*, 0 mm and 20 MHz in Figure 6c), the amplitude ratio would be severely reduced, which indicated that the signal was filtered to the greatest extent; in the meantime, the output signal phase shift approximately reached 90°, as shown in Figure 6d. All of these results could be reasonably explained according to eqs 7 and 8 and further confirmed that desired

DOI: 10.1021/acsnano.6b07446
ACS Nano 2017, 11, 882−888

signals in analog circuits with disturbance was able to be successfully screened out by the modulation of the TTD. Furthermore, a series of capacitors were used to replace the TTD to measure the amplitude ratio and phase shift, as depicted in Figure S3. As the capacitance gradually increased from 5 to 40 pF (this change was equivalent to decreasing the sliding distance), the amplitude ratio of the output voltage to the input voltage encountered a decline, while the phase shift of the output voltage increased. Consequently, all of these results displayed in Figure 6c,d and Figure S3 convincingly supported that the TTD had great potential in analog signal filtering, in place of electrically controlled tunable capacitors, and externally mechanical stimuli could be introduced to actively play a significant role in conventional analog signal modulation.

CONCLUSIONS

In summary, this paper presents a flexible TTD by coupling a TENG in a free-standing sliding mode and a variable capacitance diode. The proposed TTD can be equivalent to an external force-controlled tunable capacitor, whose capacitance is tuned by the sliding motion of a polymer film. When the sliding distance increases from 0 to 25 mm, the capacitance of the TTD declines from about 39 to 8 pF, which is extremely suitable for active analog signal modulation. When integrated into analog circuits, the TTD exhibited excellent performances in frequency modulation, phase shift, and filtering by sliding a finger. Different from previous tribotronic transistors, the TTD as a tribotronic device has demonstrated a tunable diode by the TENG for active analog signal modulation and expanded the application of the TENG as a tribo-controlled source for capacitive devices, which has great prospects in replacing ordinary variable capacitance diodes or tunable capacitors in various potential applications such as signal processing, electronic tuning circuits, precise tuning circuits, active sensor networks, phone or telephone communications, remote controls, smart wearable devices, and so on.

METHODS

Fabrication of the Flexible TTD. A polyimide (PI) substrate (100 μm thick, 20 mm × 52 mm in area) was first cleaned in an ultrasonic cleaner with deionized water, ethanol, and acetone, sequentially, and was then blow-dried in a drying oven at 120 °C for 30 min. Second, localized via holes were drilled on the PI substrate, and 10 μm thick Cu, which served as electrical wires, was deposited onto the selective area of back side of the PI substrate. Later, a layer of Ni (3 μm) was electroplated on the PI according to the designed circuit configuration to form two pads with the size of 20 × 25 mm^2, followed by the deposition of Cu (0.25 μm) to the same area. Finally, a chip of the p−n junction was adhered onto the bottom of the PI substrate, in which the anode was connected to the left Cu pad through the via hole, and the cathode was electrically connected to the right Cu pad through a 10 MΩ resistor.

Surface Modification of the PTFE Film. First, a piece of PTFE film (50 μm thick, 20 mm × 25 mm in area) was cleaned in an ultrasonic cleaner with ethanol and deionized water and was then blow-dried in a drying oven. Before being etched, a layer of Cu was sputtered onto the surface of the PTFE, and then O_2, Ar, and CF_4 gases were fed into the ICP chamber to etch the surface with flow rates of 10.0, 15.0, and 30.0 sccm, respectively. To generate the plasma, a power source of 400 W was chosen, while another power source (100 W) was used to accelerate plasma ions moving to the PTFE surface. With an etching time of 6 min, desired nanostructures were obtained on the Cu-coated PTFE surface.

Characterization and Measurement. The open-circuit voltage of the TENG was quantitatively determined by a linear motor and a system electrometer (Keithley 6514) under ambient condition at room temperature. A DC power supply (Rek RPS6003D-2) was used to supply an electrically applied reverse voltage to the tunable diode. To demonstrate the TTD's applications in analog circuits, a signal generator (AFG3102C, Tektronix) produced input signals and a mixed domain oscilloscope (MDO3024, Tektronix) analyzed the parameters of both input and output signals.

ASSOCIATED CONTENT

Supporting Information

The Supporting Information is available free of charge on the ACS Publications website at DOI: 10.1021/acsnano.6b07446.

Figures S1−S3 (PDF)
Tribotronic tuning diode for analog signal frequency modulation (Video S1) (AVI)
Tribotronic tuning diode for analog signal phase shift (Video S2) (AVI)
Tribotronic tuning diode for analog signal filtering (Video S3) (AVI)

AUTHOR INFORMATION

Corresponding Authors

*E-mail: czhang@binn.cas.cn.
*E-mail: zlwang@gatech.edu.

ORCID

Chi Zhang: 0000-0002-7511-805X
Zhong Lin Wang: 0000-0002-5530-0380

Author Contributions

§T.Z. and Z.W.Y. contributed equally to this work.

Notes

The authors declare no competing financial interest.

ACKNOWLEDGMENTS

The authors thank the National Natural Science Foundation of China (Nos. 51475099 and 51432005), Beijing Natural Science Foundation (No. 4163077), the Youth Innovation Promotion Association, CAS, the "thousands talents" program for the pioneer researcher and his innovation team, China, and National Key Research and Development Program of China (2016YFA0202704, 2016YFA0202702, 2016YFA0202703) for support.

REFERENCES

(1) Kim, C.-C.; Lee, H.-H.; Oh, K. H.; Sun, J.-Y. Highly Strechable, Transparent Inoic Touch Panel. *Science* **2016**, *353*, 682−687.
(2) Gao, W.; Emaminejad, S.; Nyein, H. Y. Y.; Challa, S.; Chen, K.; Peck, A.; Fahad, H. M.; Ota, H.; Shiraki, H.; Kiriya, D.; Lien, D.-H.; Brooks, G. A.; Davis, R. W.; Javey, A. Fully Integrated Wearable Sensor Arrays for Multiplexed in situ Perspiration Analysis. *Nature* **2016**, *529*, 509−514.
(3) Larson, C.; Peele, B.; Li, S.; Robinson, S.; Totaro, M.; Beccai, L.; Mazzolai, B.; Shepherd, R. Highly Strechable Electroluminescent Skin for Optical Signaling and Tactile Sensing. *Science* **2016**, *351*, 1071−1074.
(4) Zhou, T.; Zhang, C.; Han, C. B.; Fan, F. R.; Tang, W.; Wang, Z. L. Woven Structured Triboelectric Nanogenerator for Wearable Devices. *ACS Appl. Mater. Interfaces* **2014**, *6*, 14695−14701.
(5) Wang, C.; Hwang, D.; Yu, Z.; Takei, K.; Park, J.; Chen, T.; Ma, B.; Javey, A. User-Interactive Electronic Skin for Instantaneous Pressure Visualization. *Nat. Mater.* **2013**, *12*, 899−904.
(6) Wu, W.; Wen, X.; Wang, Z. L. Taxel-Addressable Matrix of Vertical-Nanowire Piezotronic Transistors for Active and Adaptive Tactile Imaging. *Science* **2013**, *340*, 952−957.
(7) Tang, W.; Zhou, T.; Zhang, C.; Fan, F. R.; Han, C. B.; Wang, Z. L. A Power-Transformed-and-Managed Triboelectric Nanogenerator and Its

Applications in A Self-Powered Wireless Sensing Node. *Nanotechnology* **2014**, *25*, 225402.
(8) Fan, F.-R.; Tian, Z.-Q.; Wang, Z. L. Flexible Triboelectric Generator. *Nano Energy* **2012**, *1*, 328−334.
(9) Wang, Z. L. Triboelectric Nanogenerators as New Energy Technology and Self-Powered Sensors-Principles, Problems and Perspectives. *Faraday Discuss.* **2014**, *176*, 447−458.
(10) Wang, Z. L. Triboelectric Nanogenerators as New Energy Technology for Self-Powered Systems and as Active Mechanical and Chemical Sensors. *ACS Nano* **2013**, *7*, 9533−9557.
(11) Zhang, C.; Tang, W.; Han, C.; Fan, F.; Wang, Z. L. Theoretical Comparison, Equivalent Transformation, and Conjunction Operations of Electromagnetic Induction Generator and Triboelectric Nanogenerator for Harvesting Mechanical Energy. *Adv. Mater.* **2014**, *26*, 3580−3591.
(12) Zhang, C.; Zhou, T.; Tang, W.; Han, C.; Zhang, L.; Wang, Z. L. Rotating-Disk-Based Direct-Current Triboelectric Nanogenerator. *Adv. Energy Mater.* **2014**, *4*, 1301798.
(13) Pang, Y. K.; Li, X. H.; Chen, M. X.; Han, C. B.; Zhang, C.; Wang, Z. L. Triboelectric Nanogenerators as A Self-Powered 3D Acceleration Sensor. *ACS Appl. Mater. Interfaces* **2015**, *7*, 19076−19082.
(14) Han, C. B.; Zhang, C.; Li, X. H.; Zhang, L.; Zhou, T.; Hu, W.; Wang, Z. L. Self-Powered Velocity and Trajectory Tracking Sensor Array Made of Planar Triboelectric Nanogenerator Pixels. *Nano Energy* **2014**, *9*, 325−333.
(15) Zhang, L.; Xue, F.; Du, W.; Han, C.; Zhang, C.; Wang, Z. L. Transparent Paper-Based Triboelectric Nanogenerator as A Page Mark and Anti-Theft Sensor. *Nano Res.* **2014**, *7*, 1215−1223.
(16) Tang, W.; Zhang, C.; Han, C. B.; Wang, Z. L. Enhancing Output Power of Cylindrical Triboelectric Nanogenerators by Segmentation Design and Multilayer Integration. *Adv. Funct. Mater.* **2014**, *24*, 6684−6690.
(17) Zhou, T.; Zhang, L.; Xue, F.; Tang, W.; Zhang, C.; Wang, Z. L. Multilayered Electret Films Based Triboelectric Nanogenerator. *Nano Res.* **2016**, *9*, 1442−1451.
(18) Zhang, C.; Tang, W.; Pang, Y.; Han, C.; Wang, Z. L. Active Micro-Actuators for Optical Modulation Based on A Planar Sliding Triboelectric Nanogenerator. *Adv. Mater.* **2015**, *27*, 719−726.
(19) Han, C. B.; Zhang, C.; Tian, J.; Li, X.; Zhang, L.; Li, Z.; Wang, Z. L. Triboelectrification Induced UV Emission from Plasmon Discharge. *Nano Res.* **2015**, *8*, 219−226.
(20) Zhang, C.; Tang, W.; Zhang, L.; Han, C.; Wang, Z. L. Contact Electrification Field-Effect Transistor. *ACS Nano* **2014**, *8*, 8702−8709.
(21) Zhang, C.; Wang, Z. L. Tribotronics-A New Field by Coupling Triboelectricity and Semiconductor. *Nano Today* **2016**, *11*, 521−536.
(22) Zhang, C.; Zhang, L. M.; Tang, W.; Han, C. B.; Wang, Z. L. Tribotronic Logic Circuits and Basic Operations. *Adv. Mater.* **2015**, *27*, 3533−3540.
(23) Zhang, C.; Li, J.; Han, C. B.; Zhang, L. M.; Chen, X. Y.; Wang, L. D.; Dong, G. F.; Wang, Z. L. Organic Tribotronic Transistor for Contact-Electrification-Gated Light-Emitting Diode. *Adv. Funct. Mater.* **2015**, *25*, 5625−5632.
(24) Li, J.; Zhang, C.; Duan, L.; Zhang, L. M.; Wang, L. D.; Dong, G. F.; Wang, Z. L. Flexible Organic Tribotronic Transistor Memory for a Visible and Wearable Touch Monitoring System. *Adv. Mater.* **2016**, *28*, 106−110.
(25) Pang, Y.; Xue, F.; Wang, L.; Chen, J.; Luo, J.; Jiang, T.; Zhang, C.; Wang, Z. L. Tribotronic Enhanced Photoresponsivity of a MoS_2 Phototransistor. *Adv. Sci.* **2016**, *3*, 1500419.
(26) Zhang, C.; Zhang, Z. H.; Yang, X.; Zhou, T.; Han, C. B.; Wang, Z. L. Tribotronic Phototransistor for Enhanced Photodetection and Hybrid Energy Harvesting. *Adv. Funct. Mater.* **2016**, *26*, 2554−2560.
(27) Xue, F.; Chen, L.; Wang, L.; Pang, Y.; Chen, J.; Zhang, C.; Wang, Z. L. MoS_2 Tribotronic Transistor for Smart Tactile Switch. *Adv. Funct. Mater.* **2016**, *26*, 2104−2109.
(28) Wu, J. M.; Lin, Y. H.; Yang, B.-Z. Force-Pad Made from Contact-Electrification Poly(Ethylene Oxide)/InSb Field-Effect Transistor. *Nano Energy* **2016**, *22*, 468−474.
(29) Yang, Z. W.; Pang, Y.; Zhang, L.; Lu, C.; Chen, J.; Zhou, T.; Zhang, C.; Zhong, L. W. Tribotronic Transistor Array as An Active Tactile Sensing System. *ACS Nano* **2016**, DOI: 10.1021/acsnano.6b05507.
(30) Liu, Y.; Niu, S.; Wang, Z. L. Theory of Tribotronics. *Adv. Electron. Mater.* **2015**, *1*, 1500124.
(31) Peng, W.; Yu, R.; He, Y.; Wang, Z. L. Theoretical Study of Triboelectric-Potential Gated/Driven Metal-Oxide-Semiconductor Field-Effect Transistor. *ACS Nano* **2016**, *10*, 4395−402.
(32) Niu, S.; Liu, Y.; Chen, X.; Wang, S.; Zhou, Y. S.; Lin, L.; Xie, Y.; Wang, Z. L. Theory of Freestanding Triboelectric-Layer-Based Nanogenerators. *Nano Energy* **2015**, *12*, 760−774.
(33) Jiang, T.; Chen, X.; Han, C. B.; Tang, W.; Wang, Z. L. Theoretical Study of Rotary Freestanding Triboelectric Nanogenerators. *Adv. Funct. Mater.* **2015**, *25*, 2928−2938.

DOI: 10.1021/acsnano.6b07446
ACS Nano 2017, 11, 882−888